

Remodeling of biological tissue: Mechanically induced reorientation of a transversely isotropic chain network

Ellen Kuhl
Chair for Applied Mechanics
University of Kaiserslautern, D-67653 Kaiserslautern, Germany
ekuhl@rhrk.uni-kl.de

Krishna Garikipati
Department of Mechanical Engineering,
University of Michigan, Ann Arbor, MI 48109, USA
krishna@engin.umich.edu

Ellen M. Arruda
Department of Mechanical Engineering
Macromolecular Science and Engineering Program
University of Michigan, Ann Arbor, MI 48109, USA
arruda@umich.edu

Karl Grosh
Department of Mechanical Engineering,
University of Michigan, Ann Arbor, MI 48109, USA
grosh@engin.umich.edu

October 22, 2018

Abstract

A new class of micromechanically motivated chain network models for soft biological tissues is presented. On the microlevel, it is based on the statistics of long chain molecules. A wormlike chain model is applied to capture the behavior of the collagen microfibrils. On the macrolevel, the network of collagen chains is represented by a transversely isotropic eight chain unit cell introducing one characteristic material axis. Biomechanically induced remodeling is captured by allowing for a continuous reorientation of the predominant unit cell axis driven by a biomechanical stimulus. To this end, we adopt the gradual alignment of the unit cell axis with the direction of maximum principal strain. The evolution of the unit cell axis' orientation is governed by a first-order rate equation. For the temporal discretization of the remodeling rate equation, we suggest an exponential update scheme of Euler-Rodrigues type. For the spatial discretization, a finite element strategy is applied which introduces the current individual cell orientation as an internal variable on the integration point level. Selected model problems are analyzed to illustrate the basic features of the new model. Finally, the presented approach is applied to the biomechanically relevant boundary value problem of an in vitro engineered functional tendon construct.

1 Introduction

Collagen is a fibrous protein secreted by connective tissue cells. The distinguishing feature of a typical collagen molecule is its long, stiff, triple-stranded helical structure, in which three collagen polypeptide chains, the so-called α chains, are wound around one another in a rope-like superhelix. So far, about 25 distinct collagen α chains have been identified. The α chains that make up type I collagen are by far the most common. Type I collagen is a fibril-forming collagen which is present in nearly all connective tissues such as bone, skin, tendons or ligaments. After being secreted into the extracellular space, collagen molecules assemble into collagen microfibrils. These are sparsely cross-linked higher order polymers which are about 10-300 nm in diameter and several hundreds of micrometers long, see e.g. the fundamental textbook on cell biology by Alberts et al. [1] or the rather mechanically oriented textbooks on soft biological tissues by Fung [18], Cowin & Humphrey [11], Holzapfel & Ogden [22], Humphrey [23] and Humphrey & Delange [24].

Polymer chains have many conformations of nearly equal energy. Perturbing the chains away from their equilibrium conformations typically generates entropic forces that oppose these perturbations. This is the basis for entropy based elasticity. Since the number of different configurations which a long chain molecule may assume is very large, the treatment of each of them individually would be a complex, maybe even unmanageable, task. Long chain molecules are thus commonly described by statistical mechanics, a concept which was originally developed in the context of entropic rubber elasticity by Kuhn [28,29] or Kuhn & Gr \ddot{u} n [30], see also the textbooks by Flory [14] or Treloar [43]. As pointed out by Boyce [6] and Boyce & Arruda [7], statistical, microscopically motivated models are typically characterized by a limited number of well-defined, physically-motivated material parameters. This is in contrast to the macroscopic phenomenological models documented e.g. by Ogden [37,38], Treloar [43,44] or Holzapfel [21].

Collagen chains are extremely rich in proline and glycine. While the former stabilizes the helical conformation of each α chain, the latter allows the three α chains to pack tightly together in the final collagen superhelix. Unlike polymer chains in rubber, which are of rather *uncorrelated* nature, collagen chains in biological tissues thus have to be classified as *correlated* chains from a statistical point of view. Rubber chains are typically characterized as freely jointed chains, the configuration of which resembles a random walk, whereas biological chains correspond to “wormlike chains” with a smoothly varying curvature, see Kratky & Porod [26]. Traditionally, the wormlike chain model has been applied to describe the behavior of the DNA double helix, e.g. Marko & Siggia [34] or Bustamante et al. [8]. Only recently, the wormlike chain approach has been adopted to simulate the constitutive behavior of the collagen triple helix by Bischoff et al. [4,5] and Garikipati et al. [19].

From the standpoint of polymer structures, rubber as well as soft biological tissue consists of a complex three-dimensional network of polymer chains laterally attached to one another at occasional points along their lengths. To account not only for the behavior of the individual chains as such, but also for the characteristic cross-link effects of the network structure, a number of different chain network models have been proposed over the past 60 years. The common feature of all these network models is a characteristic unit cell which is assumed to provide an adequate representation of the underlying macromolecular network structure. The existing chain network models can basically be classified in two categories: *affine* and *non-affine* models.

The first affine network model was the three chain model by James & Guth [25] and Wang & Guth [47]. Relating the overall strain state in an affine manner to the stretches of three mutually orthogonal chains, the model generally overestimates the overall stiffness when assuming that one out of these three chains is aligned with the direction of maximum principal strain. Moreover, due to the orthogonal arrangement of the three chains, cross-linking network effects are basically neglected. To remedy these deficiencies, an affine full network model was suggested by Treloar & Riding [45], compare also Wu & van der Giessen [48] or Miehe [36]. As its chains are distributed with equal probability over the solid angle, the affine full network model is considerably weaker than the three chain model since only a limited number of chains are strained up to the locking stretch upon uniaxial deformation.

The first representative of the class of non-affine models was the four chain tetrahedron model by Flory & Rehner [17] and Treloar [42]. It is not surprising though, that due to the tetrahedral shape of its unit cell, the four chain model reveals a non-physical anisotropic response. The non-affine eight chain model based on a

cubic unit cell is maybe the most prominent isotropic chain network model today, compare Arruda & Boyce [2] or Boyce [6]. Although counterintuitive at first glance, non-affine chain network models seem to be superior over affine models in predicting the overall response under various load cases as they assume an instantaneous orientation of the unit cell with respect to the principal stretch space. Critical comparisons of the different isotropic chain network models can be found in the classical textbook by Treloar [43] or in the monographs by Flory [15], Boyce & Arruda [7] or Miehe et al. [36].

It was already pointed out by Kuhn & Grün [30] that, for rubberlike materials, the assumption of isotropy is typically only met in the small strain regime. Upon further loading, the polymer chains were found to reorient themselves with respect to the loading direction. There is experimental evidence that this effect of anisotropy is even more pronounced in soft biological tissues, see e.g. the early experiments by Lanir & Fung [32], or the textbooks by Fung [18], Holzapfel & Ogden [22] and Humphrey [23]. It is widely accepted that this effect of anisotropy can be attributed to the collagenous network structure in which the polymer chains are typically oriented with respect to the predominant loading direction. A classical example is provided by Langer’s lines in skin, pointing in the direction of maximum tensile strain. Similar effects can obviously be observed in muscles, tendons and ligaments. A first attempt at modeling the anisotropic response of soft tissues based on an anisotropic eight chain unit cell has been presented recently by Bischoff et al. [3–5] and Garikipati et al. [19]. In the present work, we shall adopt the above concepts to derive a transversely isotropic chain network model, see also Kuhl et al. [27]. Following the ideas of the classical eight chain model, the isotropic in-plane response is represented in a *non-affine* manner, while the out-of-plane stretch is related to the overall macroscopic strain through an *affine* transformation.

Although characteristic for fully developed tissue, the pronounced orientation of collagen chains is typically not present in the embryonic state, see e.g. Calve et al. [9]. It is only upon mechanical loading, that the tissue exhibits a directional strengthening due the local rearrangement of the collagen fibers, an effect with is referred to as “functional adaptation” or “remodeling” in the biomechanical literature, see e.g. Taber [41]. Again, two approaches can be distinguished, macroscopic phenomenological concepts and micromechanically motivated strategies. The former are typically based on the introduction of a fictitious growth configuration and the characterization of its evolution with respect to the undeformed configuration, see e.g. Rodriguez et al. [39], Lubarda & Hoger [33], Epstein & Maugin [13] and Garikipati et al. [20]. Micromechanically motivated remodeling theories, on the contrary, are based on the rigorous reorientation of collagen fibers, see e.g. Cowin [10], Vianello [46], Sgarra & Vianello [40], Driessen et al. [12]. The present work is particularly related to the recent contribution by Menzel [35], who suggests a reorientation of the material’s principal axis with respect to the predominant loading direction.

Within this contribution, we suggest a *gradual* alignment of the axis of transverse isotropy with respect to the direction of maximum principal strain. Recall, that upon loading, the non-affine eight chain model by Arruda & Boyce [2] tacitly assumes an *instantaneous* reorientation of the representative unit cell, such that its axes always remain aligned with the principal strain axes. Herein, the approach of *instantaneous* alignment is adopted for the isotropic *non-affine* in-plane response, while for the *affine* out-of-plane response, we postulate a *gradual* reorientation.

The present manuscript is organized as follows. Section 2 introduces the basic ideas of the micromechanics of long chain molecules to simulate the individual collagen fibrils. In particular, two different types of model chains are discussed and compared: the freely jointed chain and the wormlike chain. Section 3 then deals with the mechanics of the chain network. Based on the concept of a representative eight chain unit cell, we consider a transversely isotropic network model of wormlike chain type. We then address the issue of reorientation. Accordingly, section 4 focuses on the continuum model of remodeling and its algorithmic realization. The features of the single chain model, the chain network model and the reorientation model are illustrated individually in terms of a homogeneous model problem under uniaxial tension in each section. Finally, the overall model is used to predict the fiber reorientation of randomly oriented collagen fibers in a cylindrical model tendon. The suggested remodeling approach is discussed in section 5.

Remark 1 (Notion of affinity) *Throughout this paper, we shall apply the notion of “affinity” in the context*

of “affine motion”. According to Holzapfel [21], affinity in this sense implies that changes in the length and orientation of lines marked on chains in a network are identical to changes in lines marked on the corresponding dimensions of the macroscopic sample. In the principal strain space, the eight chain model can thus be classified as an affine model. For arbitrary load cases, however, the eight chain model does not assume affine deformation of all chains, see Boyce & Arruda [7] or Miehe et al. [36]. Note that we do not use the notion of affinity in the context of “affine junction motion” which it was related to earlier in the context of constrained junction theories or phantom models, i.e. models which nicely capture the network behavior at moderate strains, see e.g. Flory & Erman [16].

2 Micromechanics of a single collagen chain

We shall begin by introducing the kinematics of a single polymer model chain. In the simplest case, this chain can be characterized through N rigid bonds of equal length l , the so-called Kuhn length, see e.g. Kuhn [28, 29]. Accordingly, the total stretched-out length of a chain, the contour length, is given as $L = Nl$. The deformation

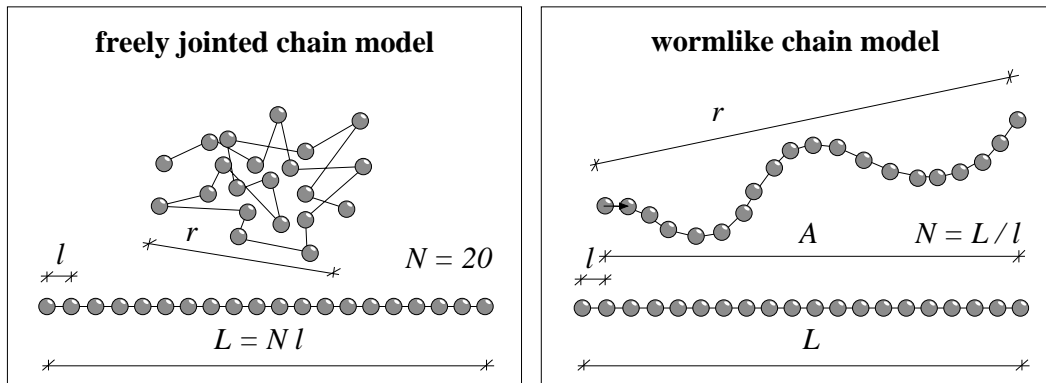


Figure 1: Kinematics of individual chain models

of this model chain is then typically defined in terms of the end-to-end distance r , i.e. the length of the vector pointing from one end of the chain to the other, whereby $0 \leq r \leq L$. Alternatively, the deformation of the chain can be characterized through the relative chain stretch $\lambda = r/L$, i.e. the dimensionless ratio between the end-to-end length and the contour length. While l , N and L are constant for a particular chain, the end-to-end length r and the chain stretch $\lambda = r/L$ change as the chain is subjected to applied forces. Two different types of chain models can be distinguished from a statistical point of view: uncorrelated and correlated chains, as illustrated in figure 1. In what follows, we will discuss different representatives of each of these classes, i.e. the classical single parameter freely jointed chain and the two parameter wormlike chain.

2.1 Uncorrelated chains: The freely jointed chain model

The most common model for chains is the random flight or rather freely jointed chain model. The freely jointed chain consists of N bonds of fixed bond length l , whereby the directions of neighboring bonds are completely uncorrelated in the sense that all directions for a given bond are of equal probability, irrespective of the directions of the neighboring segments. The model is thus characterized through one single parameter, the contour length $L = Nl$. Figure 1, left, illustrates a freely jointed chain with $N = 20$ bonds. Let us introduce the probability density $p(\lambda)$, i.e. the probability that a chain of the contour length L takes a configuration characterized through the end-to-end length r . According to the classical Boltzmann equation $s^{\text{fjc}} = k \ln(p)$, the entropy s^{fjc} of a single chain can be expressed in terms of the Boltzmann constant $k = 1.3810^{-23} \text{J/K}$ and the probability density

p . For purely entropic chains, the free energy ψ^{fjc} of a single chain can thus be expressed as $\psi^{\text{fjc}} = -k\theta \ln(p)$ where θ is the absolute temperature. Depending on the range of stretching, either Gaussian or non-Gaussian statistics are commonly applied in order to specify the particular entropy changes upon deformation. For the classical Gaussian case for which $p = p_0 \exp(-3/2 N r^2/L^2)$, the free energy of an individual chain takes the following form

$$\psi_{\text{gau}}^{\text{fjc}} = \psi_0^{\text{fjc}} + k\theta N \frac{3}{2} \frac{r^2}{L^2} \quad (1)$$

where ψ_0^{fjc} is the value of the chain energy in the unperturbed state. The single chain force follows straightforwardly as

$$f_{\text{gau}}^{\text{fjc}} = k\theta N 3 \frac{r}{L} \quad (2)$$

and is thus a linear function of the relative stretch r/L . Alternatively, we could apply non-Gaussian statistics of inverse Langevin type as introduced by Kuhn & Gr \ddot{u} n [30]. With $p = p_0 \exp(-N\mathcal{L}^{-1}r/L - N \ln(\mathcal{L}^{-1}/\sinh(\mathcal{L}^{-1})))$, the strain energy ψ^{fjc} of the freely jointed chain can be expressed as

$$\psi_{\text{lan}}^{\text{fjc}} = \psi_0^{\text{fjc}} + k\theta N \left[\frac{r}{L} \mathcal{L}^{-1} + \ln \left(\frac{\mathcal{L}^{-1}}{\sinh(\mathcal{L}^{-1})} \right) \right] \quad (3)$$

where ψ_0^{fjc} is the value of the chain energy in the unperturbed state and \mathcal{L}^{-1} is the inverse Langevin function with $\mathcal{L}(r/L) = \coth(r/L) - L/r$. Accordingly,

$$f_{\text{lan}}^{\text{fjc}} = k\theta N \mathcal{L}^{-1} \quad (4)$$

defines the force stretch relation for the freely jointed chain with inverse Langevin statistics. Recall that the inverse Langevin function can be evaluated by a Pad \acute{e} approximation as $\mathcal{L}^{-1} \approx (3 - r^2/L^2)/(1 - r^2/L^2) r/L$, as in Miehe et al. [36]. At small stretches r/L for which $\mathcal{L}^{-1} \approx 3 r/L$ the force of the inverse Langevin chain $f_{\text{lan}}^{\text{fjc}} = k\theta N \mathcal{L}^{-1}$ thus obviously approaches the force of the Gaussian chain $f_{\text{gau}}^{\text{fjc}} = k\theta N 3 r/L$.

2.2 Correlated chains: The wormlike chain model

The distinguishing feature of the wormlike chain or Kratky-Porod model chain is the continuity of the direction of its contour in space, see Kratky & Porod [26] or Flory [14]. As such, it is characterized through a smooth curvature whose direction changes randomly but in a continuous manner. This property is essentially reflected through a second parameter besides the contour length $L = Nl$, namely the persistence length A . The persistence length can be understood as the sum of the average projection of all bonds onto the direction of the first bond, as sketched in figure 1, right. Varying between $l \leq A \leq L$, the persistence length is thus a particular measure of stiffness, see also Landau & Lifshitz [31]. Accordingly, the persistence length of the uncorrelated freely jointed chain is equal to the length of the first bond $A = l$ while the persistence length of an infinitely stiff chain with almost beam-like properties is equal to its contour length $A = L$. The strain energy ψ^{wlc} of the wormlike chain model

$$\psi^{\text{wlc}} = \psi_0^{\text{wlc}} + \frac{k\theta L}{4A} \left[2 \frac{r^2}{L^2} + \frac{1}{[1 - r/L]} - \frac{r}{L} \right] \quad (5)$$

can be derived straightforwardly by integrating the force stretch relation for a wormlike chain

$$f^{\text{wlc}} = \frac{k\theta}{4A} \left[4 \frac{r}{L} + \frac{1}{[1 - r/L]^2} - 1 \right] \quad (6)$$

as originally suggested for the DNA double helix by Marko & Siggia [34] and Bustamante et al. [8] and applied for the collagen triple helix by Bischoff et al. [5]. Again, ψ_0^{wlc} is the value of the chain energy in the unperturbed state.

2.3 Example: Comparison of different chain models

To illustrate the fundamental differences between the freely jointed chain model and the wormlike chain model, we plot the different force elongation curves for two individual model chains. Figure 2, left, depicts the force elongation behavior of both, a Gaussian and an inverse Langevin freely jointed chain with the force f^{fjc} being scaled by the factor $1/[k\theta N]$. The two curves clearly monitor the deviation of Gaussian and the inverse Langevin statistics in the large strain regime, for which the linear force elongation behavior of Gaussian statistics is no longer appropriate. The inverse Langevin freely jointed chain model, however, nicely captures the characteristic locking behavior close to the locking stretch $r = L$. In the low strain region, the chain shows nearly no resistance to loading while close to its full extension, the chain stiffness increases considerably.

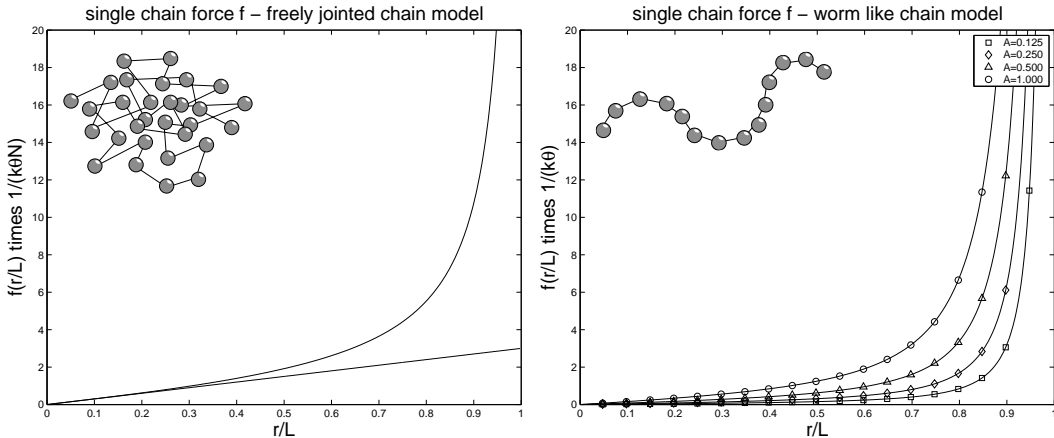


Figure 2: Force vs. elongation response of individual chain models

Next, we elaborate the force elongation response of a single wormlike chain model. Figure 2, right, shows the chain force f^{wlc} scaled by $1/[k\theta]$ for varying chain stretches r/L at different persistence lengths, A , varying from $A = 0.125$, right curve, to $A = 1.000$, left curve. Again, the characteristic locking behavior is nicely captured by the model as r/L approaches one. However, in contrast to the single parameter freely jointed chain model, the wormlike chain model offers the additional freedom of a second parameter, namely the persistence length. With this second parameter, the wormlike chain model is not only able fit the locking stretch but also to capture the shape of the force elongation curve appropriately. For larger values of of the persistence length indicating initially stiffer chains, the locking response, i.e. the behavior in the $r/L \rightarrow 1$ regime, is much smoother. For smaller values of A , the strong locking behavior of the uncorrelated freely jointed chain characterized through a steep slope of the force elongation curve can be captured.

While the freely jointed chain model of figure 2, left, shows a pronounced locking behavior, the stiffness of the wormlike chain model of figure 2, right, increases gradually as the locking stretch is approached. For the densely packed collagen fibrils considered in the present work, the two parameter wormlike chain model is believed to represent the real material behavior more accurately than the single parameter freely jointed chain model which might be better suited for randomly oriented polymer chains in rubber. In particular due to the additional freedom introduced by the persistence length as a second parameter, we shall thus focus on the wormlike chain model for the collagen fibrils in the sequel.

3 Mechanics of the chain network

To incorporate the individual chain statistics into an overall constitutive description, we apply an eight chain representation of the underlying cooperative macromolecular network structure. These eight chains are em-

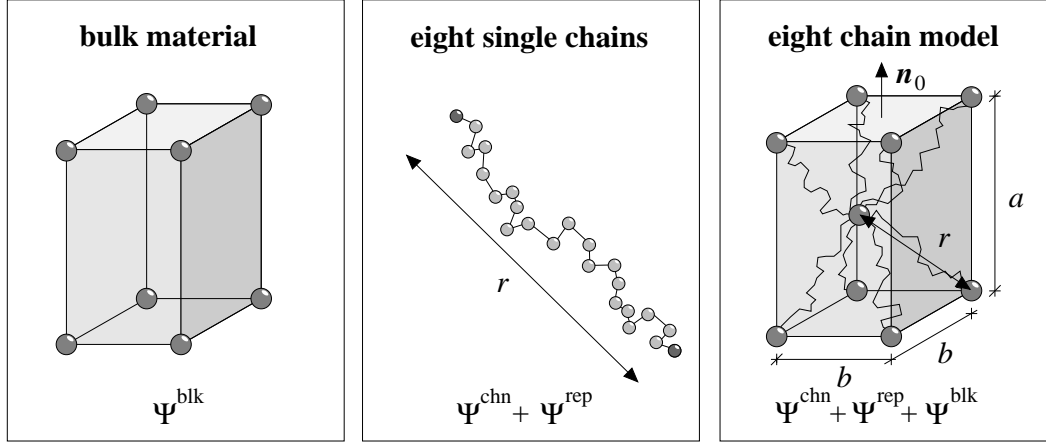


Figure 3: Kinematics of transversely isotropic eight chain network model

bedded in a transversely isotropic unit cell with initial cell dimensions a and b . They essentially link at its center and extend to the eight individual corners as in figure 3. While the end-to-end length in the undeformed configuration is obviously given as $r_0 = \sqrt{a^2 + b^2 + b^2}/2$, we assume that the end-to-end length in the deformed configuration can be expressed as

$$r = \sqrt{I_4 a^2 + [I_1 - I_4] b^2} / 2 \quad (7)$$

in terms of the first and fourth invariant I_1 and I_4 . The relevant invariants and their derivatives are given in the following form.

$$\begin{aligned} I_1 &= \mathbf{G}^{-1} : \mathbf{C} & I_3 &= \det(\mathbf{C}) & I_4 &= \mathbf{N}_0 : \mathbf{C} \\ d_{\mathbf{C}} I_1 &= \mathbf{G}^{-1} & d_{\mathbf{C}} I_3 &= I_3 \mathbf{C}^{-t} & d_{\mathbf{C}} I_4 &= \mathbf{N}_0 \end{aligned} \quad (8)$$

The first invariant I_1 can either be expressed as the trace of the covariant Cauchy Green strain tensor \mathbf{C} as $I_1 = \mathbf{G}^{-1} : \mathbf{C}$ or of the contravariant finger tensor \mathbf{b} as $I_1 = \mathbf{g} : \mathbf{b}$. Thereby, the Cauchy Green tensor \mathbf{C} is defined as the pull back of the covariant spatial metric \mathbf{g} whereas the finger tensor \mathbf{b} is the push forward of the contravariant material metric \mathbf{G}^{-1} .

$$\mathbf{C} = \mathbf{F}^t \cdot \mathbf{g} \cdot \mathbf{F} \quad \mathbf{b} = \mathbf{F} \cdot \mathbf{G}^{-1} \cdot \mathbf{F}^t \quad (9)$$

Herein, \mathbf{F} denotes the deformation gradient as $\mathbf{F} = \nabla_{\mathbf{x}} \varphi$ with φ being the deformation map between the undeformed and the deformed configuration. The determinant of either \mathbf{C} or \mathbf{b} defines the third invariant I_3 which is thus identical to the Jacobian squared $I_3 = J^2$, whereby $J = \det(\mathbf{F})$. The fourth invariant $I_4 = \lambda_a^2$ essentially represents the square of the stretch λ_a along the a direction. As such, I_4 can be expressed as the scalar product of the Cauchy Green strain \mathbf{C} with the structural tensor $\mathbf{N}_0 = \mathbf{n}_0 \otimes \mathbf{n}_0$, i.e. the dyadic product of the normal vectors \mathbf{n}_0 in the undeformed configuration. Note that while the stretch λ_a in the out-of-plane direction is captured in an *affine* way through the I_4 term, the in-plane stretch λ_b is obviously not uniquely defined. It is thus represented in a *non-affine* manner through the $[I_1 - I_4]$ term. The in-plane term $[I_1 - I_4]$ obviously results from the scalar product of \mathbf{C} with the remaining contribution $\mathbf{G}^{-1} - \mathbf{N}_0 = \mathbf{G}^{-1} - \mathbf{n}_0 \otimes \mathbf{n}_0$. Recall that in the undeformed configuration $\lambda_a = \lambda_b = 1$, $I_1 = 3$, $I_4 = 1$ and thus $r_0 = \sqrt{a^2 + b^2 + b^2}/2$. The overall energy Ψ of the transversely isotropic eight chain unit cell is assumed to consist of three contributions

$$\Psi = \Psi^{\text{blk}} + \Psi^{\text{chn}} + \Psi^{\text{rep}} \quad (10)$$

as illustrated in figure 3. The first term $\Psi^{\text{blk}}(I_1, I_3)$ captures the effect of bulk incompressibility, e.g. due to a surrounding liquid solvent, and is thus of isotropic nature, see Garikipati et al. [19]. The second term $\Psi^{\text{chn}}(I_1, I_4)$ reflects the effective assembly of the individual eight chain energies ψ^{chn} . Accordingly, $\Psi^{\text{chn}} = \gamma^{\text{chn}} \psi^{\text{chn}}$ with γ^{chn} denoting the chain density per unit cell. The repulsive term $\Psi^{\text{rep}}(I_1, I_4)$ accounts for a stress-free reference configuration and prevents the material from collapsing. The second and third terms essentially depend on the key phenomenological kinematic variable of a single chain, the current end-to-end length $r(I_1, I_4)$. For the wormlike chain model based on the free energy $\psi^{\text{chn}} = \psi^{\text{wlc}}$ according to equation (5), the individual energy terms take the following expressions,

$$\begin{aligned}\Psi^{\text{blk}} &= \gamma^{\text{blk}} \left[I_1 - 3 + \frac{1}{\beta} [I_3^{-\beta} - 1] \right] \\ \Psi^{\text{chn}} &= \frac{\gamma^{\text{chn}} k \theta L}{4A} \left[2 \frac{r^2}{L^2} + \frac{1}{[1 - r/L]^2} - \frac{r}{L} \right] \\ \Psi^{\text{rep}} &= -\frac{\gamma^{\text{chn}} k \theta}{4A} \left[\frac{1}{L} + \frac{1}{4r_0[1 - r_0/L]^2} - \frac{1}{4r_0} \right] \bar{\Psi}^{\text{rep}}\end{aligned}\quad (11)$$

where we have introduced the following abbreviation for the repulsive weighting factor $\bar{\Psi}^{\text{rep}}$.

$$\bar{\Psi}^{\text{rep}} = \ln(I_4^{[a^2 - b^2]/2}) + \frac{3}{2} \ln(I_1^{b^2}) \quad (12)$$

The parameter set of the model is thus restricted to the chain density γ^{blk} , the two wormlike chain parameters, i.e. the persistence length A and the contour length L , the cell dimensions a and b and the two bulk parameters γ^{blk} and β . The above introduced free energy Ψ defines the Kirchhoff stress $\boldsymbol{\tau}$

$$\boldsymbol{\tau} = \boldsymbol{\tau}^{\text{blk}} + \boldsymbol{\tau}^{\text{chn}} + \boldsymbol{\tau}^{\text{rep}} \quad (13)$$

as the contravariant push forward of the second Piola Kirchhoff stress $2 \text{d}_{\mathcal{C}} \Psi$ as $\boldsymbol{\tau} = \mathbf{F} \cdot 2 \text{d}_{\mathcal{C}} \Psi \cdot \mathbf{F}^t$. The individual stress contributions follow straightforwardly from the corresponding energy terms introduced in equations (11)

$$\begin{aligned}\boldsymbol{\tau}^{\text{blk}} &= \gamma^{\text{blk}} \left[2 \mathbf{b} - 2 I_3^{-\beta} \mathbf{g}^{-1} \right] \\ \boldsymbol{\tau}^{\text{chn}} &= \frac{\gamma^{\text{chn}} k \theta}{4A} \left[\frac{1}{L} + \frac{1}{4r [1 - r/L]^2} - \frac{1}{4r} \right] \bar{\boldsymbol{\tau}}^{\text{chn}} \\ \boldsymbol{\tau}^{\text{rep}} &= -\frac{\gamma^{\text{chn}} k \theta}{4A} \left[\frac{1}{L} + \frac{1}{4r_0[1 - r_0/L]^2} - \frac{1}{4r_0} \right] \bar{\boldsymbol{\tau}}^{\text{rep}}\end{aligned}\quad (14)$$

where \mathbf{g}^{-1} denotes the contravariant spatial metric. In the above equations, we have made use of the following abbreviations for the bases of the chain stress and of the repulsive stress.

$$\begin{aligned}\bar{\boldsymbol{\tau}}^{\text{chn}} &= [a^2 - b^2] \mathbf{N} + b^2 \mathbf{b} \\ \bar{\boldsymbol{\tau}}^{\text{rep}} &= \frac{1}{I_4} [a^2 - b^2] \mathbf{N} + \frac{3}{I_1} b^2 \mathbf{b}.\end{aligned}\quad (15)$$

Here, $\mathbf{N} = \mathbf{F} \cdot \mathbf{N}_0 \cdot \mathbf{F}^t$ denotes the push forward of the structural tensor \mathbf{N}_0 . As such, it can be expressed as $\mathbf{N} = \bar{\mathbf{n}} \otimes \bar{\mathbf{n}}$ in terms of the cell orientation of the deformed configuration $\bar{\mathbf{n}}_a = \mathbf{F} \cdot \mathbf{n}_a^0$. In equation (15), we have introduced the abbreviation $\bar{\boldsymbol{\tau}}^{\text{chn}} = \mathbf{F} \cdot 8r \text{d}_{\mathcal{C}} r \cdot \mathbf{F}^t$ for the derivative of the end-to-end length r . Since we assume a stress-free initial state at $r = r_0$, we conclude that $\boldsymbol{\tau}^{\text{rep}}(r_0) \doteq -\boldsymbol{\tau}^{\text{chn}}(r_0)$ and thus $\bar{\boldsymbol{\tau}}^{\text{rep}}(r_0) \doteq \bar{\boldsymbol{\tau}}^{\text{chn}}(r_0)$. Accordingly, the repulsive energy contribution $\bar{\Psi}^{\text{rep}}$ introduced in equation (11) has been constructed in such a way that $\bar{\boldsymbol{\tau}}^{\text{rep}} = \mathbf{F} \cdot 2 \text{d}_{\mathcal{C}} \bar{\Psi}^{\text{rep}} \cdot \mathbf{F}^t$. With the help of the above equations, the spatial Kirchhoff tangent $\boldsymbol{\mathcal{C}}$ relating the Lie derivative of the Kirchhoff stress $L_t \boldsymbol{\tau}$ to the Lie derivative of the covariant spatial metric $L_t \mathbf{g}$ as $L_t \boldsymbol{\tau} = \boldsymbol{\mathcal{C}} : L_t \mathbf{g} / 2$ with

$$\boldsymbol{\mathcal{C}} = \boldsymbol{\mathcal{C}}^{\text{blk}} + \boldsymbol{\mathcal{C}}^{\text{chn}} + \boldsymbol{\mathcal{C}}^{\text{rep}} \quad (16)$$

is defined through the contravariant push forward of the material tangent $4 \, \text{d}_{\mathcal{C} \otimes \mathcal{C}} \Psi$ as $\mathcal{C} = [\mathbf{F} \bar{\otimes} \mathbf{F}] : 4 \, \text{d}_{\mathcal{C} \otimes \mathcal{C}} \Psi : [\mathbf{F}^t \bar{\otimes} \mathbf{F}^t]$. Its individual contributions take the following representation.

$$\begin{aligned} \mathcal{C}^{\text{blk}} &= 4 \gamma^{\text{blk}} \left[I_3^{-\beta} \mathcal{I} + \beta I_3^{-\beta} \mathbf{g}^{-1} \otimes \mathbf{g}^{-1} \right] \\ \mathcal{C}^{\text{chn}} &= \frac{\gamma^{\text{chn}} k \theta}{64 A r^3} \left[1 - \frac{1}{1 - [1 - r/L]^2} + \frac{2r}{L [1 - r/L]^3} \right] \bar{\mathcal{C}}^{\text{chn}} \\ \mathcal{C}^{\text{rep}} &= -\frac{\gamma^{\text{chn}} k \theta}{4A} \left[\frac{1}{L} + \frac{1}{4 r_0 [1 - r_0/L]^2} - \frac{1}{4 r_0} \right] \bar{\mathcal{C}}^{\text{rep}} \end{aligned} \quad (17)$$

The fourth order basis of the chain term $\bar{\mathcal{C}}^{\text{chn}} = \bar{\tau}^{\text{chn}} \otimes \bar{\tau}^{\text{chn}}$ and of the repulsive term $\bar{\mathcal{C}}^{\text{rep}} = \mathbf{F} \cdot 2 \, \text{d}_{\mathcal{C}} \bar{\tau}^{\text{rep}} \cdot \mathbf{F}^t$ can be expressed as follows.

$$\begin{aligned} \bar{\mathcal{C}}^{\text{chn}} &= [[a^2 - b^2] \mathbf{N} + b^2 \mathbf{b}] \otimes [[a^2 - b^2] \mathbf{N} + b^2 \mathbf{b}] \\ \bar{\mathcal{C}}^{\text{rep}} &= -\frac{2}{I_1^2} [a^2 - b^2] \mathbf{N} \otimes \mathbf{N} - \frac{6}{I_1^2} b^2 \mathbf{b} \otimes \mathbf{b} \end{aligned} \quad (18)$$

In equation (17), \mathcal{I} denotes the fourth order identity which can be expressed as $\mathcal{I} = [\mathbf{g}^{-1} \bar{\otimes} \mathbf{g}^{-1} + \mathbf{g}^{-1} \otimes \mathbf{g}^{-1}] / 2$. Here, we have applied the abbreviations $\bar{\otimes}$ and \otimes for the non-standard dyadic products according to the following component-wise definitions $\{\bullet \bar{\otimes} \circ\}_{ijkl} = \{\bullet\}_{ik} \otimes \{\circ\}_{jl}$ and $\{\bullet \otimes \circ\}_{ijkl} = \{\bullet\}_{il} \otimes \{\circ\}_{jk}$. Recall that transverse isotropy is basically defined through the normal \mathbf{n}_0 of the preferred material direction. This normal will be used later on to specify biological remodeling as it is assumed to represent the orientation of collagen fibers within a tissue.

Remark 2 (Special case of an isotropic network model) *The classical non-affine isotropic eight chain model of Arruda & Boyce [2, 6, 7] which was originally introduced in the context of rubber elasticity can be understood as a special case of the present framework. Its undeformed unit cell represents a cube with $a = b$. The chain extension thus reduces to a function of the the first strain invariant I_1 such that $r = \sqrt{I_1} a/2$. For the isotropic eight chain model, the undeformed reference configuration is characterized through $\lambda_a = \lambda_b = 1$, $I_1 = 3$ and thus $r_0 = \sqrt{3} a/2$. The corresponding repulsive term $\bar{\Psi}^{\text{rep}} = 3/2 \ln(I_1^2)$ introduces the stress contributions $\bar{\tau}^{\text{chn}} = a^2 \mathbf{b}$ and $\bar{\tau}^{\text{chn}} = 3/I_1 a^2 \mathbf{b}$. Accordingly, the bases for the chain and the repulsive tangent term which follow as $\bar{\mathcal{C}}^{\text{chn}} = a^4 \mathbf{b} \otimes \mathbf{b}$ and $\bar{\mathcal{C}}^{\text{rep}} = -6 a^2 / I_1^2 \mathbf{b} \otimes \mathbf{b}$ clearly reflect the isotropic nature of this particular specification of the model.*

Remark 3 (Special case of a transversely isotropic model) *Another special case of the transversely isotropic chain network model follows from assuming a degenerated unit cell for which the in-plane dimension tends to zero as $b = 0$. This affine chain model is based on the introduction of chains which are all oriented in a single direction \mathbf{n}_0 . The deformed end-to-end length $r = \sqrt{I_4} a / 2$ thus degenerates to a mere function of the fourth invariant I_4 , or rather of the stretch λ_a , and does no longer incorporate cross-linking network effects. In the undeformed case with $I_4 = 1$, the end-to-end length is $r_0 = a / 2$. The repulsive term of equation (12) thus degenerates to $\bar{\Psi}^{\text{rep}} = \ln(I_4^{a^4/2})$. The corresponding bases of the stress and tangent contributions are then given exclusively in terms of the structural tensor \mathbf{N} as $\bar{\tau}^{\text{chn}} = a^2 \mathbf{N}$, $\bar{\tau}^{\text{rep}} = 1 / I_4 a^2 \mathbf{N}$, $\bar{\mathcal{C}}^{\text{chn}} = a^4 \mathbf{N} \otimes \mathbf{N}$ and $\bar{\mathcal{C}}^{\text{rep}} = -2 / I_4 a^2 \mathbf{N} \otimes \mathbf{N}$. Obviously, this specific representation of the model, which has been termed “decoupled reinforcement model” by Merodio and Ogden (2002), (2003) does not include the characteristic cross-link effects of the network structure.*

3.1 Example: Influence of anisotropy

In the present theory, transverse isotropy is represented by the particular initial cell orientation \mathbf{n}_0 and by the unit cell dimensions a and b . The influence of both will be studied in the sequel for the illustrative homogeneous

load case of uniaxial tension. The eight chains of the model are of wormlike chain type as introduced in section 2.2. In anticipation of later examples, the contour length L and the persistence length A have been chosen as $L = 2.125$ and $A = 1.82$. The chain density is taken as $\gamma^{\text{chn}} = 7 \times 10^{21}$. The bulk material of the unit cell is defined by the parameters $\gamma^{\text{blk}} = 100$ and $\beta = 4.5$.

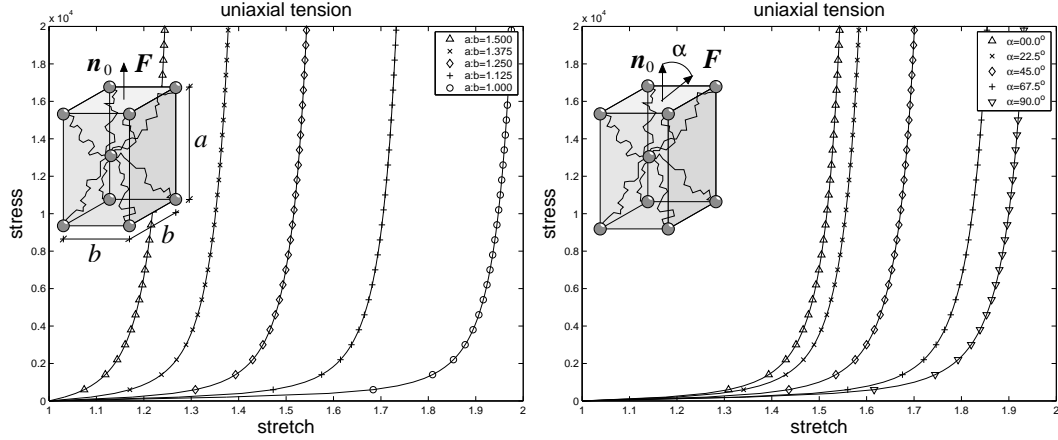


Figure 4: Influence of anisotropy – variation of cell dimensions and fiber load angle

Figure 4, left, shows the influence of the cell dimensions for different unit cell heights a with $b = 1.95$ fixed. Thereby the loading axis \mathbf{F} is aligned with the fiber direction \mathbf{n}_0 . As the cell height increases from $a = 1.95$, i.e. $a : b = 1.0$, right curve, to $a = 2.925$, i.e. $a : b = 1.5$, left curve, the material stiffens considerably. For this particular choice of parameters, the material with an aspect ratio of $a : b = 1.0$, i.e. the isotropic material, has a locking stretch which is slightly larger than $\lambda^* = 1.98$ while the locking stress of the material with $a : b = 1.5$ is close to $\lambda^* = 1.24$. Recall that at fixed contour length L , fixed persistence length A and fixed cell dimension b changes in the cell height a imply changes in the initial end-to-end length r_0 which obviously lead to changes in the overall stress strain response. The anisotropic material response is thus highly sensitive to changes in the cell dimensions.

Figure 4, right, illustrates the influence of the orientation of the fiber direction \mathbf{n}_0 with respect to the loading axis \mathbf{F} . For a fixed aspect ratio of $a : b = 1.25$ and cell dimensions $a = 2.43$ and $b = 1.95$, different fiber load angles have been studied varying from $\alpha = 0^\circ$, left curve, to $\alpha = 90^\circ$, right curve. As expected, the material stiffens as the fiber direction rotates towards the loading axis. For $\alpha = 90^\circ$, the material behaves most compliant with a locking stretch of about $\lambda^* = 1.93$, while the locking stretch of the stiffest response at $\alpha = 0^\circ$ is close to $\lambda^* = 1.55$.

3.2 Example: Anisotropic response of rabbit skin

Finally, the transversely isotropic eight chain model will be applied to simulate the behavior of skin. The following simulation is based on an experiment carried out by Lanir & Fung [32], see also Fung [18] for further details and Bischoff et al. [5] for corresponding orthotropic eight chain model simulations. In the experiment, samples of rabbit skin have been tested parallel and orthogonal to the head to tail direction. Since the collagen fibers in skin are basically oriented along the head to tail axis, the skin samples' responses were much stiffer in the head to tail direction than orthogonal to it.

With the set of parameters introduced in the previous section, $L = 2.125$, $A = 1.82$, $a = 2.43$, $b = 1.95$, $\gamma^{\text{chn}} = 7 \times 10^{21}$, $\gamma^{\text{blk}} = 100$ and $\beta = 4.5$, the transversely isotropic wormlike chain model nicely captures the experimental results by Lanir & Fung [32] which are given in figure 5, left, whereby the data points have been reproduced from the original paper. Not only the different locking stretches of about $\lambda^* = 1.55$ and $\lambda^* = 1.93$

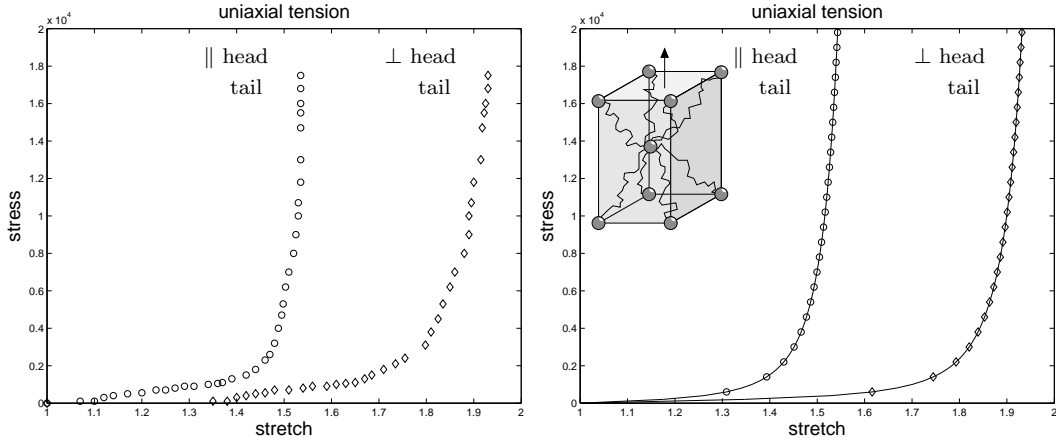


Figure 5: Anisotropy of rabbit skin – experiment vs. simulation

are captured nicely by the simulation of figure 5, right, also the overall shape of the curves corresponds to the experimental findings.

Remark 4 (Freely jointed chain network model) *Recall that the use of the freely jointed chain of section 2.1 within the eight chain network model typically overpredicts the locking behavior. Lacking the freedom of the second characteristic parameter, the freely jointed chain model experiences difficulties in simultaneously adjusting the appropriate locking stretch and the shape of the stress stretch curve. The two-parameter worm-like chain model, however, nicely captures both characteristics, not only in the single chain case but also when embedded in the representative chain network.*

4 Remodeling of the transversely isotropic tissue

Soft biological tissues such as muscles, tendons or ligaments show a pronounced orientation of collagen fibers along one or two particular directions. Nevertheless, this phenomenon which is typically not observable in neonatal tissue only develops upon mechanical loading and is often referred to as functional adaptation. In the present section, we suggest a theory that allows for a continuous redistribution of the material’s principal directions. For the transversely isotropic chain network model, we thus allow the characteristic cell axis to rotate according to a particular mechanical stimulus, in our case, the maximum principal strain.

4.1 Continuum model of remodeling

The fundamental assumption of the original isotropic eight-chain model by Arruda & Boyce [2,6,7] is that once a particular deformation is applied, the unit cell is assumed to rotate *instantaneously* towards the principal axes. The basic idea of the present model is that the unit cell axis \mathbf{n}_0 is allowed to *gradually* align with eigenvector $\mathbf{n}_\lambda^{\max}$ of Cauchy Green tensor $\mathbf{C} = \mathbf{F}^t \cdot \mathbf{g} \cdot \mathbf{F}$ which is associated with maximum eigenvalue $\lambda^{\max} = \max(\lambda_i)$. Here, $\mathbf{n}_\lambda^{\max}$ follows straightforwardly from the spectral decomposition of \mathbf{C} .

$$\mathbf{C} = \lambda_i \mathbf{n}_\lambda^i \otimes \mathbf{n}_\lambda^i \quad i = 1, 2, 3 \quad (19)$$

In some biologically relevant cases, we might encounter multiple maximum eigenvalues λ_i . For the sake of clarity, for the time being, we assume that no alignment takes place for multiple maximum eigenvalues. Following the

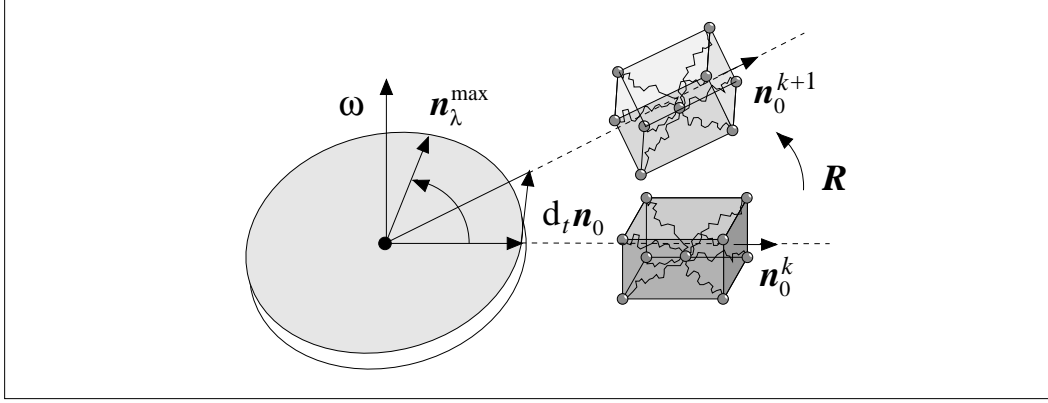


Figure 6: Reorientation with respect to principal strains

approach suggested recently by Menzel [35], we introduce the rotation vector $\boldsymbol{\omega}$

$$\boldsymbol{\omega} = \frac{1}{\tau_\omega} \mathbf{n}_0 \times \mathbf{n}_\lambda^{\max} \quad (20)$$

as the scaled vector product of the unit cell orientation \mathbf{n}_0 and the direction of the maximum principal strain $\mathbf{n}_\lambda^{\max}$ as sketched in figure 6. The decomposition of the rotation vector $\boldsymbol{\omega}$ into the unit normal \mathbf{n}^ω with $\mathbf{n}^\omega \cdot \mathbf{n}^\omega = 1$ and the magnitude ω as

$$\boldsymbol{\omega} = \omega \mathbf{n}^\omega \quad \mathbf{n}^\omega = \frac{\mathbf{n}_0 \times \mathbf{n}_\lambda^{\max}}{\|\mathbf{n}_0 \times \mathbf{n}_\lambda^{\max}\|} \quad \omega = \frac{\|\mathbf{n}_0 \times \mathbf{n}_\lambda^{\max}\|}{\tau_\omega} \quad (21)$$

illustrates, that the magnitude of rotation is obviously governed by both the time relaxation parameter τ_ω and the angle between \mathbf{n}_0 and $\mathbf{n}_\lambda^{\max}$. With the above considerations at hand, the evolution of the unit cell axis \mathbf{n}_0 can be expressed in the following abstract form

$$d_t \mathbf{n}_0 = \boldsymbol{\omega} \times \mathbf{n}_0 = -[\mathbf{e} \cdot \boldsymbol{\omega}] \cdot \mathbf{n}_0 \quad (22)$$

whereby \mathbf{e} denotes the third order permutation symbol. With the help of equation (20) the above equation can be reformulated in the following, maybe more illustrative format.

$$d_t \mathbf{n}_0 = \frac{1}{\tau_\omega} [\mathbf{n}_\lambda^{\max} - [\mathbf{n}_\lambda^{\max} \cdot \mathbf{n}_0] \mathbf{n}_0] \quad (23)$$

Note that for the particular evolution equation (22), the orthogonality condition $d_t \mathbf{n}_0 \cdot \mathbf{n}_0 = 0$ is valid throughout the remodeling history.

4.2 Discrete model of remodeling

In the present section, we suggest a discrete numerical solution strategy to solve the transient equation (23) governing the remodeling process. For its temporal discretization, consider a partition of the time interval of interest \mathcal{T} into a finite number of subintervals $\mathcal{T} = \bigcup_{k=0}^{\text{nstep}-1} [t^k, t^{k+1}]$ and focus on the typical subinterval $[t^k, t^{k+1}]$ with $\Delta t = t^{k+1} - t^k$ denoting the corresponding time increment. In doing so, we assume that the unit

cell orientation \mathbf{n}_0 is known at t^k . The suggested constitutive integrator of the evolution equation (23) is based on an exponential integration scheme which allows for a closed form representation of Euler-Rodrigues type.

$$\mathbf{n}_0^{k+1} = \exp(-\Delta t \mathbf{e} \cdot \boldsymbol{\omega}) \cdot \mathbf{n}_0^k = \mathbf{R} \cdot \mathbf{n}_0^k \quad (24)$$

In the above equation, we have introduced the proper orthogonal tensor $\mathbf{R}(\boldsymbol{\omega}) = \mathbf{R}(\boldsymbol{\omega}, \mathbf{n}^\omega)$ which is characterized through the following closed form expression.

$$\mathbf{R} = \cos(\Delta t \boldsymbol{\omega}) \mathbf{I} - \sin(\Delta t \boldsymbol{\omega}) \mathbf{e} \cdot \mathbf{n}^\omega + [1 - \cos(\Delta t \boldsymbol{\omega})] \mathbf{n}^\omega \otimes \mathbf{n}^\omega \quad (25)$$

The combination of equations (24) and (25) straightforwardly renders the following update formula for the cell axis \mathbf{n}_0^{k+1} ,

$$\mathbf{n}_0^{k+1} = \cos(\Delta t \boldsymbol{\omega}) \mathbf{n}_0^k + \sin(\Delta t \boldsymbol{\omega}) \times \mathbf{n}_0^k + [1 - \cos(\Delta t \boldsymbol{\omega})] [\mathbf{n}^\omega \cdot \mathbf{n}_0^k] \mathbf{n}^\omega \quad (26)$$

as in Menzel [35]. Recall from equation (20), that the current rotation vector $\boldsymbol{\omega} = \boldsymbol{\omega}(\mathbf{n}_0^{k+1})$ is a function of the new direction \mathbf{n}_0^{k+1} . Accordingly, the above equation is actually an implicit update equation in the unit cell direction \mathbf{n}_0^{k+1} with dependencies on \mathbf{n}_0^{k+1} on the left and righthand side. In what follows, however, we shall tacitly assume that $\mathbf{n}_0^{k+1} \times \mathbf{n}^\omega \approx \mathbf{n}_0^k \times \mathbf{n}^\omega$, such that the rotation vector $\boldsymbol{\omega}$ can be approximated as a function of the known orientation \mathbf{n}_0^k . Accordingly, $\boldsymbol{\omega}$ can then be updated explicitly as

$$\boldsymbol{\omega} = \frac{1}{\tau_\omega} \mathbf{n}_0^k \times \mathbf{n}_\lambda^{\max} \quad (27)$$

which is a reasonable assumption in the context of the gradual alignment postulated herein.

Remark 5 (Classical eight chain model) *Recall that the unit cell edges of the classical isotropic eight chain model of Arruda & Boyce [2, 6, 7] are assumed to align instantaneously with the axes of principal strain. For isotropic rubber elasticity, this might be a reasonable assumption. However, it is widely accepted that biological tissues show a gradual alignment of the material's principal axes with respect to a mechanical stimulus due to a cascade of cellular and molecular events involved in the synthesis and breakdown of collagen that occurs over time. The suggested remodeling approach inherently accounts for the successive reorientation of the anisotropic unit cell with respect to the direction of maximum principal strain. Accordingly, the final biological equilibrium state is always characterized through the alignment of the unit cell axes \mathbf{n}_0 with the maximum principal strain axes $\mathbf{n}_\lambda^{\max}$.*

4.3 Example: Influence of remodeling

The features of the suggested remodeling approach are demonstrated for the homogeneous problem under uniaxial tension illustrated in figure 7. The model parameters are adopted from the previous examples of section 3. In addition, the relaxation parameter is chosen to $\tau = 1.0$ and the time step size is $\Delta t = 0.1$. Similar to the previous examples, the specimen is loaded up to a final load of $F = 20000$ in the first ten load steps. However, now, the load is held constant for another 90 time steps to allow for a smooth adaptation of the cell orientation.

Starting at a fiber load angle of $\alpha = 90^\circ$, the cell axis \mathbf{n}_0 gradually rotates towards the loading axis, i.e. $\alpha = 0^\circ$, as time evolves, as illustrated in figure 7, left. The curves nicely demonstrate the magnitude of adaptation $\boldsymbol{\omega} = \|\mathbf{n}_0 \times \mathbf{n}_\lambda^{\max}\|/\tau_\omega$ which is obviously large for a large mismatch of axes and which decreases as the fiber load angle tends to zero. The additional influence of the relaxation parameter τ_ω manifests itself in a fast adaptation for small values of τ_ω , e.g. for $\tau_\omega = 0.5$, left curve. For larger values of τ_ω , e.g. for $\tau_\omega = 8.0$, right curve, the adaptation time increases. The suggested model is thus able to capture a gradual reorientation of the axis of transverse isotropy with respect to the principal strain axis.

The local strengthening upon reorientation is nicely documented by figure 7, right. It shows the evolution of

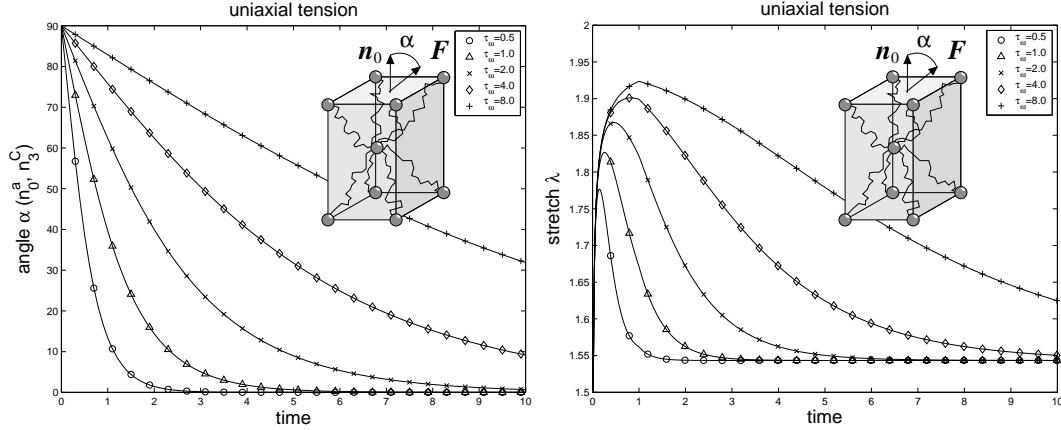


Figure 7: Remodeling – reorientation with respect to maximum principal strain axis

the stretch as a function of time. In the loading phase, the stretch increases up to about $\lambda^* = 1.93$. This value corresponds to the locking stretch of the $\alpha = 90^\circ$ orientation in figure 4, right. Then, upon remodeling, the specimen contracts as the strong material axis rotates towards the loading axis. The plateau indicates the state of biological equilibrium. The alignment of the cell axis with the axis of loading reduces the overall stretch to $\lambda^* = 1.55$ which agrees nicely with the $\alpha = 0^\circ$ results of figure 4, right.

4.4 Example: Fiber reorientation in tendons

Let us now turn to the simulation of a real biomechanical boundary value problem motivated by an experiment of engineered functional tendon constructs as documented by Calve et al. [9]. Experimental observations confirm, that in the absence of loading, the in vitro grown tendon constructs showed the typical characteristics of embryonic tendon demonstrated by the absence of a collageneous scaffold. It is only upon mechanical loading that collagen fibrils form within the tendon and orient themselves along the loading direction. The long term goal of the present project is thus to experimentally analyze and computationally predict mechanically stimulated remodeling in the form of fiber reorientation. In the future, other microstructural changes such as the increase in cross linkage or the post-depositional fusion of fibrils will be considered as well. These might be incorporated straightforwardly in the present framework through changes in the contour length or in the persistence length for which appropriate evolution equations have to be defined.

As a preliminary study, we carry out a finite element simulation of the remodeling process in a cylindrical model tendon. The tendon material is described with the transversely isotropic wormlike chain model whereby an initially random fiber orientation is assumed to represent the neonatal state. The current fiber orientation \mathbf{n}_0 is introduced as an internal variable which is stored locally on the integration point level. The tendon structure has an initial cross section of unit area and a length of twelve units, respectively. It is discretized with 2304 eight-noded brick elements introducing about 8000 degrees of freedom. The two wormlike chain parameters, i.e. the the contour length and the persistence length, take values of $L = 2.50$ and $A = 1.82$. Note that all lengths in the model are normalized by the segment length l . The bulk parameters take the values of $\gamma^{\text{blk}} = 100$ and $\beta = 4.5$, the chain density is chosen to $\gamma^{\text{chn}} = 7 \times 10^{21}$, the absolute temperature is $\theta = 310$. The dimensions of the transversely isotropic unit cell are taken as $a = 2.43$ and $b = 1.85$, again normalized with respect to the segment length l . The relaxation time for the remodeling procedure is chosen as $\tau = 1.0$.

In the first 40 time steps of $\Delta t = 0.0025$, the model tendon is gradually stretched to about 200 % of its initial length. The final load of $F = 1000$ is then held constant for another 40 time steps of $\Delta t = 0.01$ to allow for fiber reorientation, see figure 8, left. Figure 8, right, shows the temporal evolution of the elongation of the

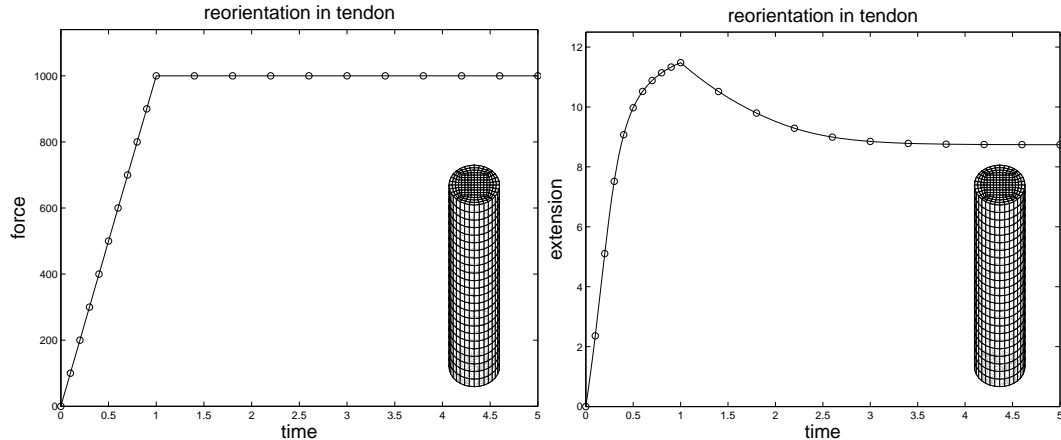


Figure 8: Remodeling of soft biological tissue – prescribed loading and extension

tendon. As the tendon is loaded, i.e. for $0.0 \leq t \leq 1.0$, the elongation increases smoothly up to almost 12 units. During the reorientation period, i.e. for $1.0 \leq t \leq 5.0$, the tendon obviously stiffens considerably due to fiber reorientation. Accordingly, the elongation reduces to about 8.5 units at the final biological equilibrium state, see figure 8, right.

Figure 9 depicts six representative stages of the remodeling history. The top figure shows the initial state at the beginning of the loading history. The arrows indicate the the initial orientation of the unit cells \mathbf{n}_0 , or, in the biomechanical sense, the directions of pronounced collagen fiber orientation, that have been assigned randomly to each individual integration point. The contour levels ranging from white to black depict the fiber load angle α varying from $\alpha = 90^\circ$, i.e. the strong cell axis being orthogonal to the loading axis, to $\alpha = 0^\circ$, i.e. a full alignment of the cell axis with the axis of loading.

Figure 9 from top to bottom nicely documents the history of remodeling. While the tendon is loaded uniaxially, a clear reorientation of the collagen fibers with respect to the loading axis can be observed. In this sense, the last figure of the series represents a biological equilibrium state, for which $d_t \mathbf{n}_0 = \mathbf{0}$. No further remodeling takes place as all fibers are aligned with the maximum principal strain direction. Accordingly, the fiber load angle indicated through the underlying contour plots evolves gradually from a random distribution in the top figure to a uniform distribution with a fiber load angle of $\alpha = 0^\circ$ in the bottom figure.

While converging towards the final biological equilibrium state the suggested procedure showed a remarkably stable algorithmic behavior. Recall that during the loading process, the tendon has been stretched to twice its original length. The stretch of the tendon as well as the remarkable reduction of its cross section are clearly visible in figure 9. The algorithm is thus able to capture both, kinematic and constitutive non-linearities. Apparently, the explicit update of the fiber direction does not lead to computational instabilities as long as the relaxation parameter is sufficiently large and the time step size is chosen sufficiently small.

5 Discussion

A new transversely isotropic chain network model has been proposed which is particularly suited to simulate remodeling of collagen fibers in soft biological tissue. For the individual chains, a wormlike chain model was adopted. In contrast to the classical uncorrelated freely jointed chain, the correlated wormlike chain shows an initial stiffness such that its curvature changes smoothly in the contour space. The stiffness, or rather the degree of correlation, is governed by a second parameter besides the contour length, the so-called persistence length. With the additional freedom of this second parameter, the wormlike chain model can capture the behavior of the freely jointed chain and a beam-like behavior as limit cases.

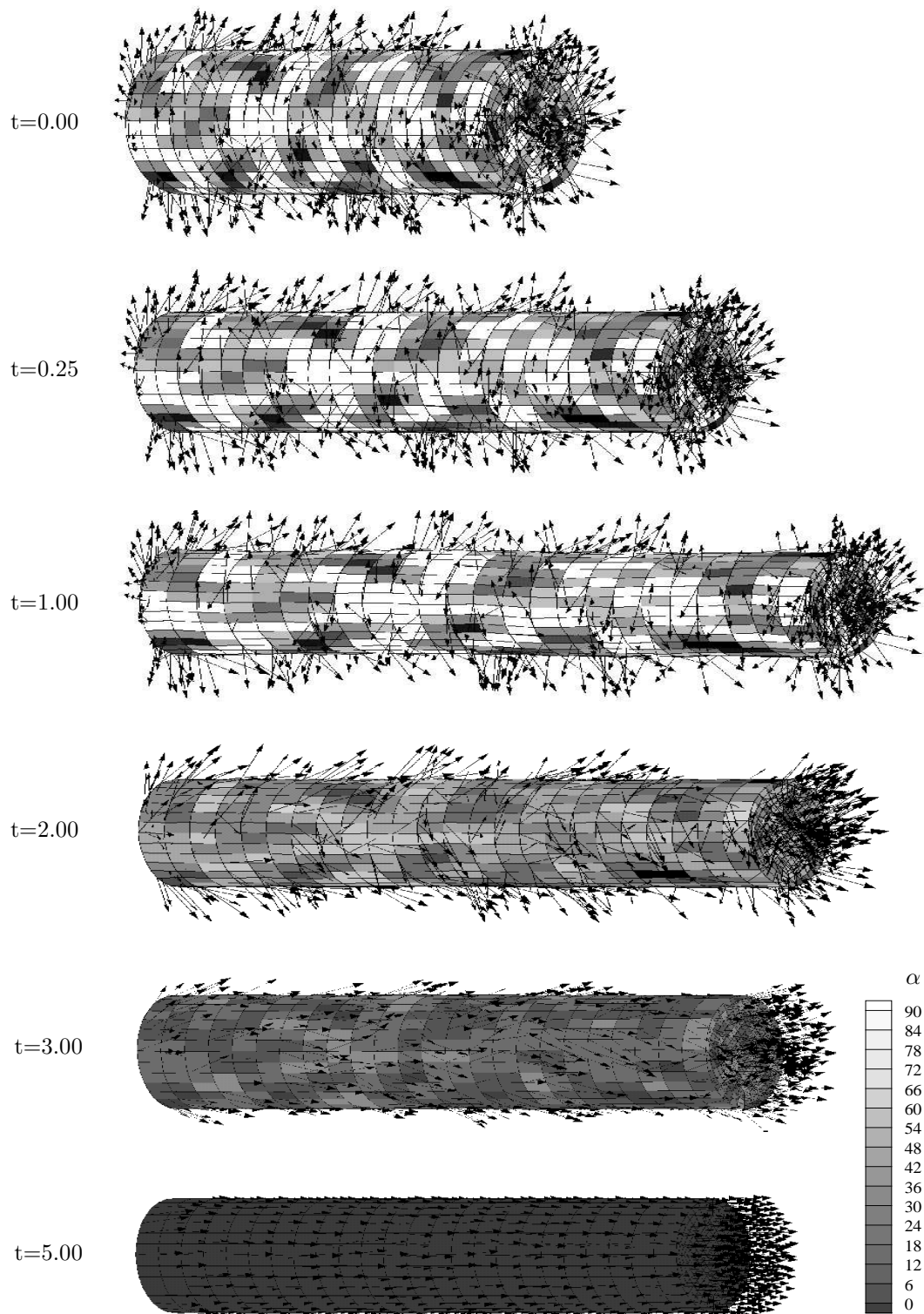


Figure 9: Remodeling of soft biological tissue – Strain based fiber reorientation of initially randomly oriented collagen fibers in a cylindrical tendon

The chain network is characterized by a representative eight chain unit cell. In contrast to the cubic cell of the isotropic eight-chain model, the present unit cell has one preferred direction which characterizes the axis of transverse isotropy. As such, the present model can be understood as a generalization of the classical eight chain model which captures the original isotropic eight chain model as a special limit case with equal cell dimensions. In the other limit, i.e. when the in-plane dimensions of the unit cell tend to zero, the model captures the effects of unidirectional fiber reinforcement neglecting cross-link effects of the network structure.

To incorporate biomechanical remodeling, the characteristic axis of the transversely isotropic unit cell was allowed to rotate with respect to a biological stimulus, in our case the maximum principal strain axis. A theoretical framework of remodeling and its numerical realization based on an exponential update scheme of Euler-Rodrigues type have been introduced. Thereby, the characteristic unit cell axis has been introduced as an internal variable on the integration point level of a finite element realization.

A first comparison of the suggested approach with the experimental findings of in vitro engineered tendon constructs revealed a remarkably good agreement. Being essentially based on micromechanical considerations, the present model is governed by a limited number of physically-motivated material parameters. As such, it is believed to be ideally suited to simulate not only the passive behavior of soft biological tissues but also their active response to changes in the mechanical loading environment.

References

- [1] ALBERTS, B., A. JOHNSON, J. LEWIS, M. RAFF, K. ROBERTS & P. WALTER [2002]. *Molecular biology of the cell*. Garland Science, Taylor & Francis Group, New York.
- [2] ARRUDA, E. M. & M. C. BOYCE [1993]. ‘A three-dimensional constitutive model for the large stretch behavior of rubber elastic materials.’ *J. Mech. Phys. Solids*, **41**, pp. 389–412.
- [3] BISCHOFF, J. E., E. M. ARRUDA & K. GROSH [2000]. ‘Finite element modeling of human skin using an isotropic, nonlinear elastic constitutive model.’ *J. Biomechanics*, **33**, pp. 645–652.
- [4] BISCHOFF, J. E., E. M. ARRUDA & K. GROSH [2002]. ‘A microstructurally based orthotropic hyperelastic constitutive lay.’ *J. Appl. Mech.*, **69**, pp. 570–579.
- [5] BISCHOFF, J. E., E. M. ARRUDA & K. GROSH [2002]. ‘Orthotropic hyperelasticity in terms of an arbitrary molecular chain model.’ *J. Appl. Mech.*, **69**, pp. 198–201.
- [6] BOYCE, M. C. [1996]. ‘Direct comparison of the Gent and the Arruda-Boyce models of rubber elasticity.’ *Rubber Chem. Technol.*, **69**, pp. 781–785.
- [7] BOYCE, M. C. & E. M. ARRUDA [2000]. ‘Constitutive models of rubber elasticity: A review.’ *Rubber Chem. Technol.*, **73**, pp. 504–523.
- [8] BUSTAMANTE, C., Z. BRYANT & S. B. SMITH [2003]. ‘Ten years of tension: single-molecule DNA mechanics.’ *Nature*, **421**, pp. 423–427.
- [9] CALVE, S., R. G. DENNIS, P. E. KOSNIK, K. BAAR, K. GROSH & E. M. ARRUDA [2004]. ‘Engineering of functional tendon.’ *Tissue Engineering, in press*.
- [10] COWIN, S. C. [1995]. ‘Optimization of the strain energy density in linear anisotropic elasticity.’ *J. Elasticity*, **34**, pp. 45–68.
- [11] COWIN, S. C. & J. D. HUMPHREY [2001]. *Cardiovascular Soft Tissue Mechanics*. John Wiley & Sons, Chichester – New York.

- [12] DRIESSEN, N. J. B., G. W. M. PETERS, J. M. HUGHE, C. V. C. BOUTEN & F. P. T. BAAIJENS [2003]. ‘Remodelling of continuously distributed collagen fibres in soft connective tissue.’ *J. Biomechanics*, **36**, pp. 1151–1158.
- [13] EPSTEIN, M. & G. A. MAUGIN [2000]. ‘Thermomechanics of volumetric growth in uniform bodies.’ *Int. J. Plasticity*, **16**, pp. 951–978.
- [14] FLORY, P. J. [1969]. *Statistical Mechanics of Chain Molecules*. John Wiley & Sons, Chichester – New York.
- [15] FLORY, P. J. [1976]. ‘Statistical thermodynamics of random networks.’ *Proceedings of the Royal Society of London A*, **351**, pp. 351–378.
- [16] FLORY, P. J. & B. ERMAN [1982]. ‘Theory of elasticity of polymer networks.’ *Macromolecules*, **15**, pp. 800–806.
- [17] FLORY, P. J. & J. REHNER [1943]. ‘Statistical mechanics of cross-linked polymer networks.’ *J. Chem. Phys.*, **11(11)**, pp. 512–520.
- [18] FUNG, Y. C. [1993]. *Biomechanics – Mechanical Properties of Living Tissues*. Springer Verlag, Berlin – Heidelberg – New York, second edition.
- [19] GARIKIPATI, K., E. M. ARRUDA, K. GROSH, H. NARAYANAN & S. CALVE [2004]. ‘A continuum treatment of growth in biological tissue: The coupling of mass transport and mechanics.’ *J. Mech. Phys. Solids*, **52**, pp. 1595–1625.
- [20] GARIKIPATI, K., H. NARAYANAN, E. M. ARRUDA, K. GROSH & S. CALVE [2004]. ‘Material forces in the context of bio-tissue remodelling.’ In *Mechanics of material forces*, edited by P. Steinmann & G. A. Maugin. Kluwer Academic Publishers.
- [21] HOLZAPFEL, G. A. [2000]. *Nonlinear Solid Mechanics: A Continuum Approach for Engineering*. John Wiley & Sons.
- [22] HOLZAPFEL, G. A. & R. W. OGDEN [2003]. *Biomechanics of Soft Tissue in Cardiovascular Systems*. CISM Courses and Lectures No. 441, Springer Verlag, Wien – New York.
- [23] HUMPHREY, J. D. [2002]. *Cardiovascular Solid Mechanics*. Springer Verlag, Berlin – Heidelberg – New York.
- [24] HUMPHREY, J. D. & S. L. DELANGE [20024]. *An Introduction to Biomechanics*. Springer Verlag, Berlin – Heidelberg – New York.
- [25] JAMES, H. M. & E. GUTH [1943]. ‘Theory of elastic properties of rubber.’ *J. Chem. Phys.*, **11(10)**, pp. 455–481.
- [26] KRATKY, O. & G. POROD [1949]. ‘Röntgenuntersuchungen gelöster Fadenmoleküle.’ *Recueil Trav. Chim.*, **68**, pp. 1106–1122.
- [27] KUHLE, E., A. MENZEL & K. GARIKIPATI [2004]. ‘On the convexity of transversely isotropic chain network models.’ *Phil. Mag.*, *submitted for publication*.
- [28] KUHN, W. [1934]. ‘Über die Gestalt fadenförmiger Moleküle in Lösungen.’ *Kolloid-Zeitschrift*, **52**, pp. 2–15.
- [29] KUHN, W. [1936]. ‘Beziehungen zwischen Molekülgröße, statistischer Molekülgestalt und elastischen Eigenschaften hochpolymerer Stoffe.’ *Kolloid-Zeitschrift*, **76**, pp. 258–271.

- [30] KUHN, W. & F. GRÜN [1942]. ‘Beziehungen zwischen elastischen Konstanten und Dehnungsdoppelbrechung hochelastischer Stoffe.’ *Kolloid-Zeitschrift*, **101**, pp. 248–271.
- [31] LANDAU, L. D. & E. M. LIFSHITZ [1951]. *A Course on Theoretical Physics, Volume 5, Statistical Physics, Part I*. Butterworth Heinemann (reprint).
- [32] LANIR, Y. & Y. C. FUNG [1974]. ‘Two-dimensional mechanical properties of rabbit skin – II Experimental results.’ *J. Biomechanics*, **7**, pp. 171–182.
- [33] LUBARDA, V. A. & A. HOGER [2002]. ‘On the mechanics of solids with a growing mass.’ *Int. J. Solids & Structures*, **39**, pp. 4627–4664.
- [34] MARKO, J. F. & E. D. SIGHA [1995]. ‘Stretching DNA.’ *Macromolecules*, **28**, pp. 8759–8770.
- [35] MENZEL, A. [2004]. ‘Modeling of anisotropic growth in biological tissues – A new approach and computational aspects.’ *Biomechanics and Modeling in Mechanobiology*, *in press*.
- [36] MIEHE, C., S. GÖKTEPE & F. LULEI [2004]. ‘A micro-macro approach to rubber-like materials – Part I: The non-affine micro-sphere model of rubber elasticity.’ *J. Mech. Phys. Solids*, **52**, pp. 2617–2660.
- [37] OGDEN, R. W. [1972]. ‘Large deformation isotropic elasticity – On the correlation of theory and experiment for incompressible rubberlike solids.’ *Proceedings of the Royal Society of London A*, **326**, pp. 565–584.
- [38] OGDEN, R. W. [1984]. *Non-Linear Elastic Deformations*. Ellis Horwood, Chichester.
- [39] RODRIGUEZ, E. K., A. HOGER & A. D. MC CULLOCH [1994]. ‘Stress-dependent finite growth in soft elastic tissues.’ *J. Biomechanics*, **27**, pp. 455–467.
- [40] SGARRA, C. & M. VIANELLO [1997]. ‘Rotations which make strain and stress coaxial.’ *J. Elasticity*, **47**, pp. 217–224.
- [41] TABER, L. A. [1995]. ‘Biomechanics of growth, remodeling, and morphogenesis.’ *ASME Appl. Mech. Rev.*, **48**, pp. 487–545.
- [42] TRELOAR, L. R. G. [1946]. ‘The elasticity of a network of long-chain molecules.’ *Trans. Faraday Soc.*, **42**, pp. 83–94.
- [43] TRELOAR, L. R. G. [1975]. *The Physics of Rubber Elasticity*. Clarendon Press – Oxford.
- [44] TRELOAR, L. R. G. [1976]. ‘The mechanics of rubber elasticity.’ *Proceedings of the Royal Society of London A*, **351**, pp. 301–330.
- [45] TRELOAR, L. R. G. & G. RIDING [1979]. ‘A non-Gaussian theory for rubber in biaxial strain. I. mechanical properties.’ *Proceedings of the Royal Society of London A*, **369**, pp. 261–280.
- [46] VIANELLO, M. [1996]. ‘Coaxiality of strain and stress in anisotropic linear elasticity.’ *J. Elasticity*, **42**, pp. 283–289.
- [47] WANG, M. C. & E. GUTH [1952]. ‘Statistical theory of networks on non-Gaussian flexible chains.’ *J. Chem. Phys.*, **20**(7), pp. 1144–1157.
- [48] WU, P. D. & E. VAN DER GIESSEN [1993]. ‘On improved network models for rubber elasticity and their applications to orientation hardening in glassy polymers.’ *J. Mech. Phys. Solids*, **41**, pp. 427–456.